THE JOURNAL OF PHYSICAL CHEMISTRY A

Article

Cite This: J. Phys. Chem. A 2018, 122, 7514−7521

pubs.acs.org/JPCA

Time-Dependent Density-Functional Theory for Modeling Solid-State Fluorescence Emission of Organic Multicomponent Crystals

Mihails Arhangelskis,*[,†,‡] Dominik B. Jochym,[§] Leonardo Bernasconi,[§] Tomislav Friščić,[‡] Andrew J. Morris,*[,∥] and William Jones[†]

[†]Department of Chemistry, University of Cambridge, Lensfield Road, Cambridge CB2 1EW, United Kingdom

[‡]Department of Chemistry, McGill University, 801 Sherbrooke Street W., Montreal H3A 0B8, Québec, Canada

[§]STFC Rutherford Appleton Laboratory, Didcot OX11 0QX, United Kingdom

[∥]School of Metallurgy and Materials, University of Birmingham, Edgbaston, Birmingham B15 2TT, United Kingdom

Supporting Information

ABSTRACT: We describe the approach for modeling solid-state fluorescence spectra of organic crystalline materials, using the recent implementation of time-dependent density-functional theory within the plane-wave/pseudopotential code CASTEP. The method accuracy is evaluated on a series of organic cocrystals displaying a range of emission wavelengths. In all cases the calculated spectra are in good to excellent agreement with experiment. The ability to precisely model the emission spectra offers novel insight into the role of intermolecular interactions and crystal packing on solid-state luminescence of organic chromophores, allowing the possibility of *in silico* design of organic luminescent materials.

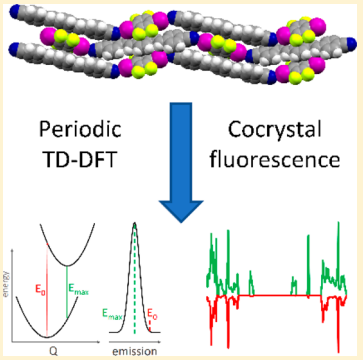

INTRODUCTION

Organic luminescent materials are very important due to their application in the production of light-emitting diodes, lasers,[1,2] sensors,[3] dyes,[4] and pigments.[5] They provide opportunities for constructing novel devices, such as curved multicolor displays,[6] tunable dye lasers,[7] and organic solar cells.[8] With such a broad range of applications, the ability to tune or at least model the luminescence of an organic material remains a challenge of considerable importance. One of the promising approaches for the design of materials with modified colors[9−11] and tunable luminescent properties[12−14] is cocrystal formation, i.e., the formation of multicomponent crystals composed of a molecular fluorophore in combination with one or more cocrystal former (coformer) molecules. As the interaction between the fluorescent building block and the coformer is based on complementary supramolecular interactions (e.g., halogen[15] or hydrogen bonding, $\pi\cdots\pi$ stacking, etc.), cocrystallization enables the synthesis of libraries of multiple fluorescent materials based on the same emissive component. Importantly, different coformers will lead to the formation of different crystal structures. This provides a unique opportunity to place a fluorescent emissive component into different solid-state environments, thereby allowing the fine-tuning of the fluorescent emission properties. However, this approach to generation of emissive organic solids is largely based on trial-and-error experiment, since the relationship between the optical and luminescent properties of these materials and their crystal structure is poorly understood. The development of novel luminescent cocrystals, therefore, remains based on screening multiple chromophore−coformer combinations in order to achieve a material with desirable properties.

Recently, our team, and others, has demonstrated the use of molecular[16,17] and periodic[9,18] density-functional theory (DFT) to rationalize the colors of organic crystalline solids, including cocrystals. However, specific modeling and prediction of emissive properties of crystalline solids also necessitate the consideration of their time-dependent electronic behavior.[19] This requires the implementation of time-dependent density-functional theory (TD-DFT), a rapidly developing area whose emerging potential has so far been used to address problems such as exciton behavior,[20] optical absorption,[21] dynamics of photoexcited polymers,[22] and photoelectron spectroscopy.[23]

We now present the use of a plane-wave implementation of TD-DFT based on Hutter's linear response formalism[24] for highly accurate modeling and prediction of the luminescent emission of organic crystalline materials, using as model systems the recently reported highly emissive cocrystals of 1,4-bis(2-cyanostyryl)benzene (**A**).[12] Importantly, we previously demonstrated that halogen bond-driven cocrystallization[25] of **A** with halogen bond donors, including 1,4-diiodobenzene (**1**), 1,4-diiodo- (**2**), and 1,4-dibromotetrafluorobenzene (**3**), as

Received: April 12, 2018
Revised: August 15, 2018
Published: August 30, 2018

DOI: 10.1021/acs.jpca.8b03481
J. Phys. Chem. A 2018, 122, 7514−7521

well as 4-bromo-tetrafluorobenzoic acid (**4**), results in new materials whose fluorescent emission maxima are significantly shifted compared to pure crystalline **A** (Figure 1). Through the use of TD-DFT modeling code described below, we are now able to model and explain, for the first time, the luminescent behavior of such multicomponent organic materials. Hitherto, and before the introduction of periodic TD-DFT, the modeling of luminescence spectra of crystalline materials was based on molecular clusters extracted from known crystal structures.[26,27] Although such an approach can, in principle, yield accurate results, it is important to ensure that the cluster is sufficiently large to adequately mimic the periodic environments found within crystals. In contrast, calculations in a periodic plane-wave basis set are inherently free of complications associated with such limitations. It will be shown that highly accurate emission wavelengths can be calculated by performing periodic calculations on primitive cells, making for an affordable and straightforward algorithm for calculating solid-state fluorescence spectra.

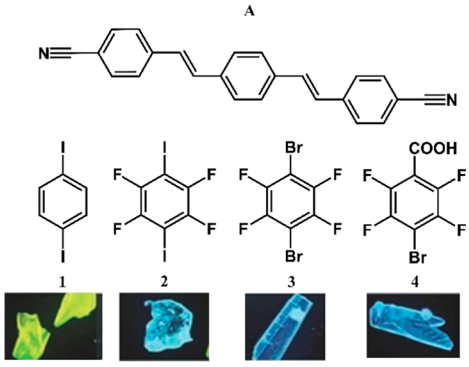

Figure 1. Molecular structures of compound **A** and coformers **1**–**4**. The colors of the corresponding cocrystals under UV light are shown underneath the molecular structures.[12]

THEORY

Periodic DFT algorithms can be divided into two categories, namely, those using localized all-electron basis sets and those utilizing the plane-wave approach with core pseudopotentials. The same division extends to the time-dependent domain. TD-DFT with localized basis sets has been implemented within the code CRYSTAL,[28,29] where it has been used to model optical properties of metals[30] and semiconductors.[31] Herein we present the recently developed implementation of periodic TD-DFT in a plane-wave code CASTEP and illustrate its capabilities by modeling solid-state fluorescence spectra of organic multicomponent crystals.

The TD-DFT algorithm used in CASTEP follows Hutter's implementation[24] based on linear response using the Tamm–Dancoff approximation (TDA).[32] In the TDA, occupied–virtual contributions (see eq. 17 in Hutter[24]) are disregarded while retaining the virtual–occupied ones, since the contribution from the former is assumed small. In their implementation, Hutter reformulated the equations of time-dependent Hartree–Fock (TD-HF) theory such that they could be efficiently implemented in codes using a plane-wave basis set. The TD-HF equations are non-Hermitian eigenvalue equations which are solved, in CASTEP, using a preconditioned block Davidson solver.[33] Hutter's original formulation assumed that the special k-point gamma is used. In this work we have used an extension of Hutter's derivation to a single arbitrary k-point. Such an extension was made possible by using a complex representation of the response density. Geometry optimization in the excited state was performed using forces obtained according to procedures described in CASTEP development reports.[34]

Occasionally TD-DFT calculations produce so-called "spurious" excited states, which do not correspond to any physical excitation processes.[35] In the Hutter formulation of linear-response TD-DFT for plane-waves, the operator diagonalized to determine the excitation energies can be split into two parts, one corresponding to the Kohn–Sham eigenvalue difference and the other arising from applying a response potential to the ground-state wave function. Solutions of the matrix equations that provide a pure Kohn–Sham orbital transition, with no contribution from the exchange-correlation terms, are considered spurious.

The use of hybrid functionals with TD-DFT is a straightforward extension to local functionals within CASTEP with the addition of a HF-like response term. We note that using purely HF exchange for TD-DFT in the TDA is equivalent to CIS (configuration interaction with single substitutions).[36]

As a first step of our calculations, we performed ground-state geometry optimizations of the different crystal structures using a semilocal GGA-type PBE[37] functional combined with Grimme D2 dispersion correction.[38] In this process we allowed full relaxation of atom coordinates as well as unit cell parameters, subject only to the symmetry constraints of their respective space groups. The unit cell parameters obtained in this step were then fixed for the remainder of the calculation of the fluorescence spectra. This was required due to inability of the current CASTEP TD-DFT implementation to calculate stress tensors and perform variable cell optimization. The limitation, however, was deemed an acceptable approximation, since molecular crystals are not expected to undergo significant unit cell distortions upon electronic excitation.

Following the ground-state geometry optimization, it was then necessary to decide on how to treat Brillouin zone (BZ) sampling for the excited-state TD-DFT calculations. When performing periodic total energy calculations, it is necessary to integrate over the entire BZ. This integral is commonly approximated by weighted averaging over certain "k-points", usually at high-symmetry points within the BZ. In the case of Hutter's TD-DFT implementation,[24] we were limited to the use of a single k-point, which is generally insufficient to obtain accurate excited-state energies in solids. Creating a suitably large supercell was, computationally, prohibitively expensive due to the cost of periodic TD-DFT calculations for large simulation cells. We therefore turned our attention to the idea of a mean-value k-point, as proposed by Baldereschi.[39] In this approach an optimum single k-point representing the average of the entire Brillouin zone can be found for each crystal lattice. Indeed, calculations using this mean-value k-point are expected to provide results closer to those obtained with a converged k-point grid at a fraction of the computational cost. In order to verify the validity of this approach, we have calculated the emission spectrum of the **A:1** cocrystal using a mean-value k-point, as well as the high-symmetry gamma k-point. Indeed, the mean-value approach provides far better agreement with experiment (Supporting Information Figure S1). The details of our procedures for selecting the mean-value

DOI: 10.1021/acs.jpca.8b03481
J. Phys. Chem. A 2018, 122, 7514–7521

k-point and calculating the fluorescence spectra are described in the Supporting Information.

The oscillator strengths were calculated using Tamm−Dancoff approximation;[40,41] therefore, these values could only be used for qualitative selection of the excited states with greatest contribution to the emission spectra. For the triclinic structure **A:1**, only the first electronic excited state showed a large oscillator strength, resulting in a single band in the emission spectrum. The monoclinic unit cells of the isostructural cocrystals **A:2**, **A:3**, and **A:4** contain two molecules of **A**[12] leading to pairs of nearly degenerate electronic bands, HOCO-1 with HOCO and LUCO with LUCO+1. Transitions between these bands resulted in the formation of two distinct electronic excited states S_1 and S_3 accompanied by a spurious[42−44] state S_2. Based on the oscillator strengths, the S_3 electronic state was found to give the largest contribution to the emission spectrum (for details see Supporting Information section 2.2.4).

The selected excited states were geometry-optimized to account for Stokes shift resulting from the vibrational relaxation of the electronic excited states following electronic excitation. Additionally, it was necessary to consider the limitations of plane-wave DFT with regard to hybrid functionals. It is known that hybrid functionals (e.g., PBE0,[45,46] B3LYP,[47,48] or HSE06[49]) provide more accurate band gap values[50,51] and excitation energies[21,41] compared to local and semilocal functionals. Unfortunately, the computational cost of plane-wave DFT codes, with hybrid functionals,[52] compared to localized basis set implementations makes it impractical to use these functionals for geometry optimization within TD-DFT. In order to achieve higher accuracy at a lower computational cost, we performed TD-DFT geometry optimizations using PBE[37] functional combined with Grimme D2 dispersion correction.[38] The PBE optimizations were followed by single-point B3LYP calculations to obtain a correction to the electronic band gap beyond PBE.

We note that the addition of a small amount of Hartree−Fock exchange (such as found in HSE, B3LYP, or PBE0) has been shown to improve the spectral properties and geometries of excited states in periodic TD-DFT calculations. PBE alone does not renormalize the Coulomb term in the response equations leading to an incorrect long-range tail (corresponding to $G = 0$ in reciprocal space).[53] This results in poor performance of PBE with extended covalent systems, such as graphene,[54] which must be treated with hybrid TD-DFT to obtain reasonable geometries of electronic excited states. Hybrid functionals show improved behavior in the $G \rightarrow 0$ limit due to the contribution of Hartree−Fock (HF) exchange. The materials in our study, however, are molecular crystals held together via comparatively weak noncovalent interactions, which makes the effect of PBE long-range error less significant for the excited-state geometries.

As a verification for the correctness of the geometries of PBE-optimized excited states, we compared the geometrical changes occurring in crystal structures during TD-DFT geometry optimization with the corresponding gas-phase calculation. The gas-phase TD-DFT calculation was performed in Gaussian 16[55] using a hybrid B3LYP functional. Consistency between periodic PBE and gas-phase B3LYP geometrical parameters is expected to serve as a good indicator for the validity of our periodic TD-DFT methodology.

In order to validate the excitation energies calculated with B3LYP hybrid functional (20% Hartree−Fock exchange), we have performed additional TD-DFT single-point calculations with PBE0 (25% HF exchange) and TD-HF calculations (Supporting Information section 1.2.4, Tables S14−S22). The excitation energies predicted by PBE0 were generally 0.1−0.2 eV higher than their B3LYP counterparts but showed consistency in terms of band populations. The TD-HF calculations were not expected to produce accurate excitation energies. Indeed, they overestimate hybrid TD-DFT energies by 1 eV or more. The purpose of these calculations was to verify the ordering of excited states in terms of band populations. In that regard TD-B3LYP, TD-PBE0, and TD-HF calculations showed consistency with respect to the lowest energy excited states used for modeling the fluorescence spectra.

In order to assess the role of cocrystal coformers on the formation of electronic excited states, we have performed density of states (DOS) and projected density of states (PDOS), as well as band structure (BS) calculations. These calculations were performed in CASTEP using PBE functional, and the DOS plots were calculated with OptaDOS[56,57] code. Since the PBE functional is known to underestimate the calculated band gaps as well as generate unphysical low-energy charge-transfer states, we have also calculated BS plots with a hybrid B3LYP functional. Since calculations involving HF exchange are computationally inefficient in plane-wave formalism, we have used CRYSTAL14[28] periodic DFT code with localized basis sets for this purpose.

Further details of the calculations, including the selection of mean-value k-points for each crystal structure, parameters of ground-state and TD-DFT periodic geometry optimizations, as well as the methodology for gas-phase calculations, are provided in the Supporting Information.

RESULTS AND DISCUSSION

Comparison of measured cocrystal fluorescence spectra (Figure 2) and fluorescence lifetimes[12] for **A**, **A:1**, **A:2**, **A:3**, and **A:4** reveals significant variation of emissive behavior depending on the coformer choice. In particular, **A:1** displays green fluorescence similar to that observed for pure compound **A**, while also showing a similar fluorescence lifetime of ∼20 ns. On the other hand, cocrystals containing fluorinated coformers **A:2**, **A:3**, and **A:4**, exhibit blue emission with a much shorter emission lifetime (∼1 ns). Additionally, the emission line shapes of the materials are considerably different: the green-emitting **A:1** cocrystal has a bell-shaped emission line, while the **A:2**−**A:4** materials produce emission spectra with three

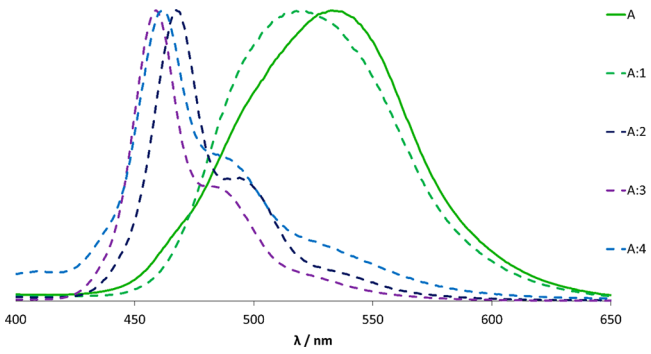

Figure 2. Fluorescence spectra of compound **A** and its cocrystals **A:1**−**A:4**. Data acquired from Yan et al.[12]

DOI: 10.1021/acs.jpca.8b03481
J. Phys. Chem. A 2018, 122, 7514−7521

maxima, which are likely caused by a vibrational progression characteristic of polyaromatic molecules.[58,59] Two potential explanations for the observed differences in emission behavior of the cocrystals may be offered. First, the variations in fluorescence emission may result from differences in orbital overlap between the molecules of **A** and those of the coformers. It may be speculated that the nonfluorinated coformer **1** and fluorinated coformers **2**−**4** have different HOMO and LUMO energies, causing variations in fluorescence emission.

Alternatively, changes in fluorescence emission might be explained by the effect of different arrangements of **A** itself, e.g., due to changes in $\pi-\pi$ stacking interactions between molecules of **A**. In order to decide between these two possibilities, we conducted TD-DFT modeling of fluorescence spectra for all four cocrystal structures.[12] Cocrystal **A:1** crystallizes in a triclinic unit cell with a centrosymmetric space group *P*-1. The chromophore molecules **A** form $\pi-\pi$ stacking interactions with neighboring chromophore molecules. In these stacks each molecule is offset by ∼2/3 of its length relative to the nearest neighbors, which is illustrated in Figure 3 , top. The mutually isostructural cocrystals **A:2**, **A:3**, and **A:4** crystallize in a monoclinic space group $P2_1/n$. Crystal packing diagrams (Figure 3, bottom) reveal that chromophore molecules in these structures are offset sideways, greatly reducing the overlap between the neighboring π systems. The lack of $\pi-\pi$ stacking interactions in the monoclinic cocrystals may account for the blue shift in fluorescence emission compared to the triclinic cocrystal **A:1**.

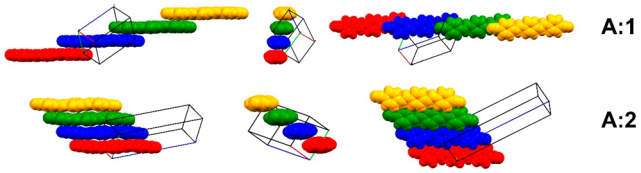

Figure 3. Molecular packing diagrams of **A:1** triclinic structure and **A:2** monoclinic structure (bottom). Each structure is shown in three different orientations, and different colors are used for clarity. In the triclinic **A:1** structure chromophore molecules form partially overlapping $\pi-\pi$ stacks, while in the monoclinic structure **A:2** chromophore molecules show no stacking interactions.

The calculated fluorescence spectra are in good agreement with experiment (Figure 4), with the absolute error in calculated emission maxima always less than 0.2 eV. Such an accuracy of periodic TD-DFT calculations was sufficient to correctly predict the emission color, which is of major practical importance for the computational design of organic luminescent materials.

Having successfully modeled the fluorescence spectra, we next turned our attention to a rationalization of the origin of the different fluorescence behavior of the cocrystals. Our first hypothesis was that the blue shift in fluorescence emission of **A:2**, **A:3**, and **A:4** cocrystals results from orbital mixing between the chromophore and coformer molecules. The density of states (DOS) calculations, performed using OptaDOS[56,57] code, however, showed that in all cases such orbital mixing is insignificant (Supporting Information Figures S3−S10). An alternative explanation may be provided by considering variations in crystal packing. Indeed, π stacking is present in cocrystal **A:1** (mean stacking distance 3.5 Å), whereas the **A**−**A** interplanar distances in the isostructural cocrystals **A:2**, **A:3**, and **A:4** are approximately 7 Å, thereby resulting in very little π stacking interactions (Figure 3).

Such stacking differences are unexpected given that coformers **1**−**4** are similar in size and contain two halogen/hydrogen bond donors at 180° orientation. In order to evaluate the role of crystal packing, therefore, TD-DFT calculations were performed on hypothetical crystal structures created by (a) replacing the coformers in the monoclinic cell of **A:2**, **A:3**, or **A:4** with coformer **1** and (b) replacing the coformer in the triclinic cell of **A:1** with **2**, **3**, and **4**. Calculations for the hypothetical monoclinic **A:1** structure indicated a blue shift compared to the experimental triclinic structure (λ_{max} 419 with a maximum in the violet-blue region), while hypothetical triclinic structures for **A:2**, **A:3**, and **A:4**

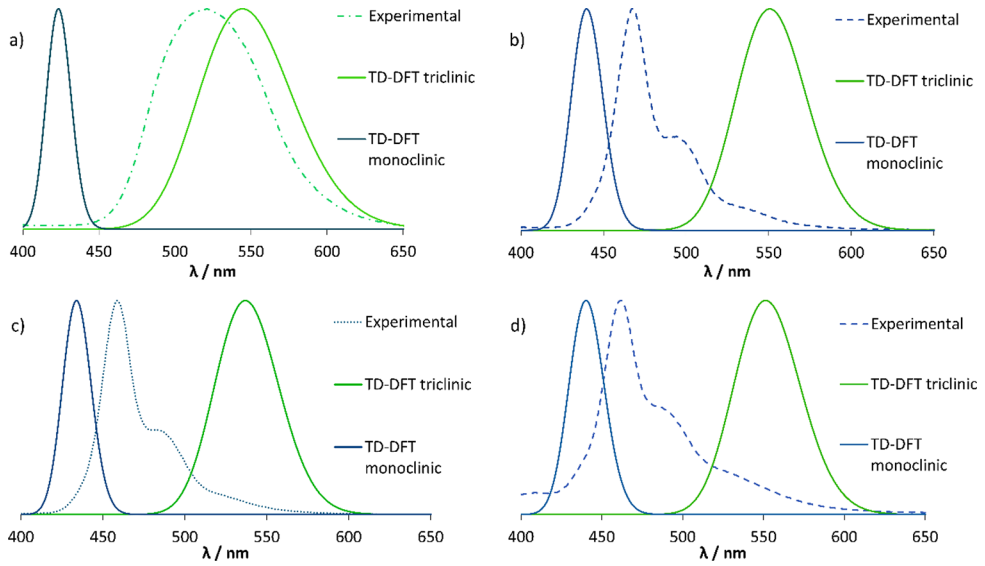

Figure 4. Experimental and calculated spectra fluorescence spectra: (a) **A:1**, (b) **A:2**, (c) **A:3**, and (d) **A:4**. Experimental spectra are shown with dashed/dotted lines, while spectra calculated with TD-DFT/B3LYP are shown with solid lines. The colors of the spectral lines were calculated from the corresponding spectra using the ProPhoto RGB color space.

DOI: 10.1021/acs.jpca.8b03481
J. Phys. Chem. A 2018, 122, 7514−7521

showed green fluorescence with λ_{max} 550, 537, and 551 nm, respectively. The resulting calculations, therefore, unambiguously indicated that it is the crystal packing which is responsible for the fluorescence behavior of the experimental cocrystals. We note that nature of the coformer, however, does determine the relative thermodynamic stability of the experimental and hypothetical structures. Ground-state periodic DFT lattice energy calculations showed that the triclinic structure is lowest in energy for **A:1**, while the monoclinic structures are preferred for **A:2**, **A:3**, and **A:4**—results indeed in agreement with the experimentally observed crystal structures (Table 1).

Table 1. Calculated Relative Lattice Energies of Triclinic and Monoclinic Crystal Structures[a]

	relative energy/kJ mol^{-1}	
cocrystal	triclinic	monoclinic
A:1	**0.0**	19.0
A:2	22.5	**0.0**
A:3	28.9	**0.0**
A:4	15.1	**0.0**

[a]It is evident that experimentally observed polymorphs (triclinic for **A:1** and monoclinic for **A:2**, **A:3**, and **A:4**) are lowest in energy for each cocrystal type.

The differences in $\pi-\pi$ stacking arrangements are also the likely reason for differences in line shapes of the triclinic and monoclinic structures. To investigate this effect, we have calculated fluorescence emission spectrum of an isolated molecule **A**. The calculation was performed in Gaussian 16[55] software at the TD-DFT/B3LYP level of theory with a 6-311G(d,p) basis set. Vibrational eigenvectors and frequencies were calculated for electronic ground and excited states, and vibrational line shapes were evaluated within the Franck–Condon approximation. The calculated emission spectrum of an isolated molecule **A** contains a vibrational progression closely resembling the line shapes of the monoclinic cocrystals **A:2**–**A:4** which lack $\pi-\pi$ stacking interactions (Figure 5).

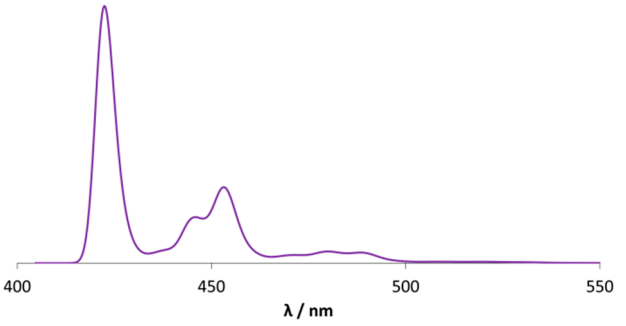

Figure 5. Calculated S_1 emission spectrum of molecule **A** in the gas phase, qualitatively resembling the solid-state fluorescence line shapes of cocrystals **A:2**–**A:4**.

Calculation of fluorescence line shape for the structures containing $\pi-\pi$ interactions would require constructing a molecular cluster, making the calculation prohibitively expensive and unfeasible. With further developments in the periodic TD-DFT approach we shall be able to perform excited-state phonon calculations and explore the effects of crystal packing on the emission line shape.

As a further validation of our TD-DFT calculations, we have calculated band structures and band gaps using the B3LYP hybrid functional within a localized triple-ζ basis set specially modified for periodic calculations (pob-TZVP),[60] as implemented in the periodic DFT code CRYSTAL14.[28] These calculations allowed us to verify that TD-DFT excitation energies mirror the energies of the unperturbed Kohn–Sham states. In particular, the calculations show that the energies of S_1 excited states at the ground-state molecular geometry are in good agreement with the calculated band gaps (Table S31).

As a final validation of our method, we compared the effect of electronic excitation on the geometry of molecule **A** in solid state and in the gas phase. The plots of HOMO and LUMO orbitals of the chromophore molecule (Figure 6) reveal

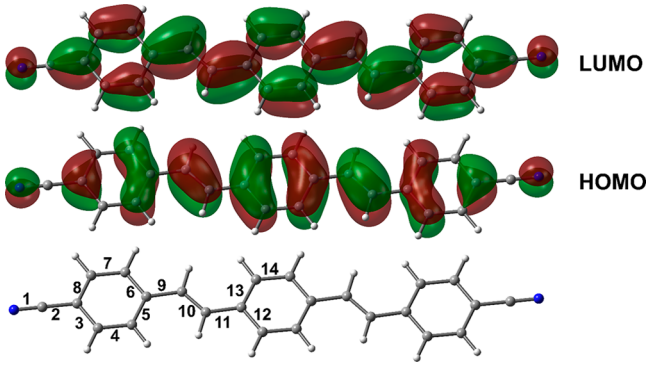

Figure 6. Plots of HOMO and LUMO orbitals of molecule **A**, as well as the bond numbering scheme used in Table 2. Since the molecule is centrosymmetric, only half of the bonds were labeled. The bonds experiencing increased bonding character in the LUMO are expected to shorten upon electronic excitation, while bonds getting more antibonding character are expected to elongate.

alternating regions of bonding and antibonding electron density. We may therefore expect a particular trend for bond length alternations in the π system of the chromophore: the bonds experiencing an increase in bonding character are expected to shorten upon excitation, while the bonds with increased antibonding character shall elongate. The analysis of bond length variations in triclinic **A:1** and monoclinic **A:2** cocrystal structures as well as gas-phase molecule **A** meet these expectations perfectly (Table 2). This is particularly gratifying since the cocrystal geometry optimizations were performed with a PBE functional, while the molecular calculation was done using a hybrid B3LYP functional. This result proves that semilocal periodic TD-DFT calculations offer a correct description of electronic excitations in cocrystal structures. It is interesting to note that bond variations for the monoclinic **A:2** structure are approximately half of those for the triclinic **A:1** structure. We believe this has to do with the different number of molecules in the corresponding crystal structures. The triclinic **A:1** cell contains one chromophore molecule, while the monoclinic **A:2** cell contains two such molecules. The periodic TD-DFT calculation involves excitation of one electron per unit cell; therefore, each molecule in the monoclinic cell is effectively excited by half an electron, leading to smaller geometrical variations between the ground and excited states.

DOI: 10.1021/acs.jpca.8b03481
J. Phys. Chem. A 2018, 122, 7514–7521

Table 2. Effect of Electronic Excitation on the Equilibrium Geometry of Molecule A in the Triclinic Structure A:1 and Monoclinic Structure A:2 as Well as in the Gas Phase[a]

	bond lengths/Å								
	A:1 triclinic			A:2 monoclinic			isolated molecule		
bond no.	ground	excited	difference	ground	excited	difference	ground	excited	difference
1	1.165	1.170	+0.005	1.165	1.167	+0.002	1.156	1.158	+0.002
2	1.426	1.419	−0.007	1.424	1.421	−0.003	1.429	1.422	−0.007
3	1.415	1.424	+0.009	1.416	1.421	+0.005	1.405	1.411	+0.006
4	1.389	1.384	−0.005	1.389	1.386	−0.003	1.383	1.378	−0.005
5	1.417	1.430	+0.013	1.419	1.425	+0.006	1.409	1.423	+0.014
6	1.416	1.427	+0.011	1.416	1.422	+0.006	1.407	1.420	+0.013
7	1.390	1.385	−0.005	1.390	1.387	−0.003	1.386	1.379	−0.007
8	1.411	1.423	+0.012	1.413	1.419	+0.006	1.401	1.411	+0.010
9	1.454	1.434	−0.020	1.456	1.445	−0.011	1.461	1.435	−0.026
10	1.359	1.384	+0.025	1.360	1.375	+0.015	1.347	1.375	+0.028
11	1.453	1.431	−0.022	1.452	1.439	−0.013	1.460	1.432	−0.028
12	1.417	1.430	+0.013	1.419	1.427	+0.008	1.408	1.422	+0.014
13	1.416	1.433	+0.017	1.416	1.425	+0.009	1.406	1.427	+0.021
14	1.389	1.380	−0.009	1.389	1.384	−0.005	1.384	1.374	−0.010

[a]The elongation and contraction of C−C bonds is consistent with the positions of the nodes in the HOMO and LUMO π orbitals.

CONCLUSIONS

To summarize, we have provided the first demonstration of how periodic TD-DFT calculations can be used to accurately predict solid-state fluorescence spectra of organic crystalline materials. We have rationalized the blue shift in fluorescence emission of monoclinic cocrystals **A:2**−**A:4** as being caused by the lack of π−π stacking interactions between neighboring **A** molecules. The differences in stacking arrangements between triclinic and monoclinic cocrystals were also linked to the changes in atomic vibrational motion and, consequently, fluorescence line shapes. Finally, we have shown how the nature of cocrystal chromophore may be used to control the intermolecular arrangements of the chromophore molecules, causing significant changes to the emission wavelength.

We believe that our work bridges the gap between crystal structure and solid-state fluorescence emission and provides a strategy for efficient theory-driven design of novel luminescent materials.

ASSOCIATED CONTENT

Supporting Information

The Supporting Information is available free of charge on the ACS Publications website at DOI: 10.1021/acs.jpca.8b03481.

Details of the computational procedures, including the derivation of mean-value k-points, TD-DFT excitation energies which were used in computing the fluorescence spectra, DOS, and band structure plots (additional data related to this publication are available from the University of Cambridge data repository: https://doi.org/10.17863/CAM.11545) (PDF)

AUTHOR INFORMATION

Corresponding Authors

*E-mail: mihails.arhangelskis@mcgill.ca.
*E-mail: A.J.Morris.1@bham.ac.uk.

ORCID

Mihails Arhangelskis: 0000-0003-1150-3108
Leonardo Bernasconi: 0000-0002-9460-7975
Tomislav Friščić: 0000-0002-3921-7915
Andrew J. Morris: 0000-0001-7453-5698
William Jones: 0000-0002-4690-4852

Notes

The authors declare no competing financial interest.

ACKNOWLEDGMENTS

M.A. thanks EPSRC for a Ph.D. studentship. A.J.M. acknowledges the support from the Winton Program for the Physics of Sustainability. We are grateful for computational support from the U.K. national high-performance computing service, ARCHER, for which access was obtained via the UKCP consortium and funded by EPSRC grant ref EP/K013564/1. Computing resources for DFT calculations with CRYSTAL code were provided by STFC Scientific Computing Department's SCARF cluster. Compute Canada (www.computecanada.ca) and WestGrid (www.westgrid.ca) are acknowledged for the use of Cedar supercomputer to perform Gaussian calculations. Dr. Dongpeng Yan is thanked for providing experimental fluorescence spectra.

REFERENCES

(1) Gao, F.; Liao, Q.; Xu, Z.-Z.; Yue, Y.-H.; Wang, Q.; Zhang, H.-L.; Fu, H.-B. Strong Two-Photon Excited Fluorescence and Stimulated Emission from an Organic Single Crystal of an Oligo(Phenylene Vinylene). *Angew. Chem., Int. Ed.* **2010**, *49*, 732−735.

(2) Yan, D.; Evans, D. G. Molecular Crystalline Materials with Tunable Luminescent Properties: From Polymorphs to Multi-Component Solids. *Mater. Horiz.* **2014**, *1*, 46−57.

(3) Zou, X.; Zhu, G.; Hewitt, I. J.; Sun, F.; Qiu, S. Synthesis of a Metal−organic Framework Film by Direct Conversion Technique for VOCs Sensing. *Dalt. Trans.* **2009**, 3009−3013.

(4) Pu, Y.-J.; Higashidate, M.; Nakayama, K.; Kido, J. Solution-Processable Organic Fluorescent Dyes for Multicolor Emission in Organic Light Emitting Diodes. *J. Mater. Chem.* **2008**, *18*, 4183−4188.

(5) Dreuw, A.; Plötner, J.; Lorenz, L.; Wachtveitl, J.; Djanhan, J. E.; Brüning, J.; Metz, T.; Bolte, M.; Schmidt, M. U. Molecular Mechanism of the Solid-State Fluorescence Behavior of the Organic Pigment Yellow 101 and Its Derivatives. *Angew. Chem., Int. Ed.* **2005**, *44*, 7783−7786.

(6) Weaver, M. S.; Hewitt, R. H.; Kwong, R. C.; Mao, S. Y.; Michalski, L. A.; Ngo, T.; Rajan, K.; Rothman, M. A.; Silvernail, J. A.;

DOI: 10.1021/acs.jpca.8b03481
J. Phys. Chem. A 2018, 122, 7514−7521

Bennet, W. D.; et al. Flexible Organic Light-Emitting Devices. *Proc. SPIE* **2001**, 113−119.
(7) Bañuelos, J.; Martín, V.; Gómez-Durán, C. F. A.; Córdoba, I. J. A.; Peña-Cabrera, E.; García-Moreno, I.; Costela, Á.; Pérez-Ojeda, M. E.; Arbeloa, T.; Arbeloa, Í. L. New 8-Amino-BODIPY Derivatives: Surpassing Laser Dyes at Blue-Edge Wavelengths. *Chem. - Eur. J.* **2011**, *17*, 7261−7270.
(8) Hiramoto, M.; Fujiwara, H.; Yokoyama, M. Three-Layered Organic Solar Cell with a Photoactive Interlayer of Codeposited Pigments. *Appl. Phys. Lett.* **1991**, *58*, 1062−1064.
(9) Sander, J. R. G.; Bučar, D.-K.; Henry, R. F.; Baltrusaitis, J.; Zhang, G. G. Z.; MacGillivray, L. R. A Red Zwitterionic Co-Crystal of Acetaminophen and 2,4-Pyridinedicarboxylic Acid. *J. Pharm. Sci.* **2010**, *99*, 3676−3683.
(10) Arhangelskis, M.; Lloyd, G. O.; Jones, W. Mechanochemical Synthesis of Pyrazine:Dicarboxylic Acid Cocrystals and a Study of Dissociation by Quantitative Phase Analysis. *CrystEngComm* **2012**, *14*, 5203−5208.
(11) Sangtani, E.; Sahu, S. K.; Thorat, S. H.; Gawade, R. L.; Jha, K. K.; Munshi, P.; Gonnade, R. G. Furosemide Cocrystals with Pyridines: An Interesting Case of Color Cocrystal Polymorphism. *Cryst. Growth Des.* **2015**, *15*, 5858−5872.
(12) Yan, D.; Delori, A.; Lloyd, G. O.; Friščić, T.; Day, G. M.; Jones, W.; Lu, J.; Wei, M.; Evans, D. G.; Duan, X. A Cocrystal Strategy to Tune the Luminescent Properties of Stilbene-Type Organic Solid-State Materials. *Angew. Chem., Int. Ed.* **2011**, *50*, 12483−12486.
(13) Yan, D.; Delori, A.; Lloyd, G. O.; Patel, B.; Friščić, T.; Day, G. M.; Bučar, D.-K.; Jones, W.; Lu, J.; Wei, M.; et al. Modification of Luminescent Properties of a Coumarin Derivative by Formation of Multi-Component Crystals. *CrystEngComm* **2012**, *14*, 5121−5123.
(14) Feng, Q.; Wang, M.; Dong, B.; He, J.; Xu, C. Regulation of Arrangements of Pyrene Fluorophores via Solvates and Cocrystals for Fluorescence Modulation. *Cryst. Growth Des.* **2013**, *13*, 4418−4427.
(15) Fox, D.; Metrangolo, P.; Pasini, D.; Pilati, T.; Resnati, G.; Terraneo, G. Site-Selective Supramolecular Synthesis of Halogen-Bonded Cocrystals Incorporating the Photoactive Azo Group. *CrystEngComm* **2008**, *10*, 1132−1136.
(16) Sangtani, E.; Mandal, S. K.; Sreelakshmi, A. S.; Munshi, P.; Gonnade, R. G. Salts and Cocrystals of Furosemide with Pyridines: Differences in π-Stacking and Color Polymorphism. *Cryst. Growth Des.* **2017**, *17*, 3071−3087.
(17) Feng, H.-T.; Xiong, J.-B.; Luo, J.; Feng, W.-F.; Yang, D.; Zheng, Y.-S. Selective Host-Guest Co-Crystallization of Pyridine-Functionalized Tetraphenylethylenes with Phthalic Acids and Multicolor Emission of the Co-Crystals. *Chem. - Eur. J.* **2017**, *23*, 644−651.
(18) Arhangelskis, M.; Eddleston, M. D.; Reid, D. G.; Day, G. M.; Bučar, D.-K.; Morris, A. J.; Jones, W. Rationalization of the Color Properties of Fluorescein in the Solid State: A Combined Computational and Experimental Study. *Chem. - Eur. J.* **2016**, *22*, 10065−10073.
(19) Runge, E.; Gross, E. K. U. Density-Functional Theory for Time-Dependent Systems. *Phys. Rev. Lett.* **1984**, *52*, 997−1000.
(20) Yang, Z.; Ullrich, C. A. Direct Calculation of Exciton Binding Energies with Time-Dependent Density-Functional Theory. *Phys. Rev. B: Condens. Matter Mater. Phys.* **2013**, *87*, 195204.
(21) Bernasconi, L.; Webster, R.; Tomić, S.; Harrison, N. M. Optical Response of Extended Systems from Time-Dependent Hartree-Fock and Time-Dependent Density-Functional Theory. *J. Phys. Conf. Ser.* **2012**, *367*, 012001.
(22) Bernasconi, L. Chaotic Soliton Dynamics in Photoexcited Trans -Polyacetylene. *J. Phys. Chem. Lett.* **2015**, *6*, 908−912.
(23) De Giovannini, U.; Hübener, H.; Rubio, A. A First-Principles Time-Dependent Density Functional Theory Framework for Spin and Time-Resolved Angular-Resolved Photoelectron Spectroscopy in Periodic Systems. *J. Chem. Theory Comput.* **2017**, *13*, 265−273.
(24) Hutter, J. Excited State Nuclear Forces from the Tamm-Dancoff Approximation to Time-Dependent Density Functional Theory within the Plane Wave Basis Set Framework. *J. Chem. Phys.* **2003**, *118*, 3928−3934.
(25) Cavallo, G.; Metrangolo, P.; Pilati, T.; Resnati, G.; Sansotera, M.; Terraneo, G. Halogen Bonding: A General Route in Anion Recognition and Coordination. *Chem. Soc. Rev.* **2010**, *39*, 3772−3783.
(26) Lukeš, V.; Polovková, J.; Rapta, P.; Végh, D. The Experimental and Theoretical Characterisation of the Phenyl-Perfluorophenyl Π−π and Hydrogen Bond Interactions in the Aldimine Co-Crystal. *Chem. Phys.* **2006**, *326*, 271−280.
(27) Gatti, T.; Brambilla, L.; Tommasini, M.; Villafiorita-Monteleone, F.; Botta, C.; Sarritzu, V.; Mura, A.; Bongiovanni, G.; Del Zoppo, M. Near IR to Red Up-Conversion in Tetracene/Pentacene Host/Guest Cocrystals Enhanced by Energy Transfer from Host to Guest. *J. Phys. Chem. C* **2015**, *119*, 17495−17501.
(28) Dovesi, R.; Orlando, R.; Erba, A.; Zicovich-Wilson, C. M.; Civalleri, B.; Casassa, S.; Maschio, L.; Ferrabone, M.; De La Pierre, M.; D'Arco, P.; et al. CRYSTAL14 : A Program for the *Ab Initio* Investigation of Crystalline Solids. *Int. J. Quantum Chem.* **2014**, *114*, 1287−1317.
(29) Dovesi, R.; Erba, A.; Orlando, R.; Zicovich-Wilson, C. M.; Civalleri, B.; Maschio, L.; Rérat, M.; Casassa, S.; Baima, J.; Salustro, S.; et al. Quantum-Mechanical Condensed Matter Simulations with CRYSTAL. *Wiley Interdiscip. Rev. Comput. Mol. Sci.* **2018**, *8*, e1360.
(30) Webster, R.; Bernasconi, L.; Harrison, N. M. Optical Properties of Alkali Halide Crystals from All-Electron Hybrid TD-DFT Calculations. *J. Chem. Phys.* **2015**, *142*, 214705.
(31) Bernasconi, L.; Tomić, S.; Ferrero, M.; Rérat, M.; Orlando, R.; Dovesi, R.; Harrison, N. M. First-Principles Optical Response of Semiconductors and Oxide Materials. *Phys. Rev. B: Condens. Matter Mater. Phys.* **2011**, *83*, 1−7.
(32) Fetter, A. L.; Walecka, J. D. *Quantum Theory of Many-Particle Systems*; McGraw-Hill: New York, 1971.
(33) Davidson, E. R. The Iterative Calculation of a Few of the Lowest Eigenvalues and Corresponding Eigenvectors of Large Real-Symmetric Matrices. *J. Comput. Phys.* **1975**, *17*, 87−94.
(34) Jochym, D. B. *Hybrid Time-Dependent Density Functional Theory in CASTEP: A DCSE Project Part 2: Atomic Forces in Excited Electronic States*; 2012.
(35) Heßelmann, A.; Görling, A. Blindness of the Exact Density Response Function to Certain Types of Electronic Excitations: Implications for Time-Dependent Density-Functional Theory. *Phys. Rev. Lett.* **2009**, *102*, 233003.
(36) Jochym, D. B. *Hybrid Time-Dependent Density Functional Theory in CASTEP: A DCSE Project*; 2010.
(37) Perdew, J. P.; Burke, K.; Ernzerhof, M. Generalized Gradient Approximation Made Simple. *Phys. Rev. Lett.* **1996**, *77*, 3865−3868.
(38) Grimme, S. Semiempirical GGA-Type Density Functional Constructed with a Long-Range Dispersion Correction. *J. Comput. Chem.* **2006**, *27*, 1787−1799.
(39) Baldereschi, A. Mean-Value Point in the Brillouin Zone. *Phys. Rev. B* **1973**, *7*, 5212−5215.
(40) Hirata, S.; Head-Gordon, M. Time-Dependent Density Functional Theory within the Tamm−Dancoff Approximation. *Chem. Phys. Lett.* **1999**, *314*, 291−299.
(41) Sander, T.; Maggio, E.; Kresse, G. Beyond the Tamm-Dancoff Approximation for Extended Systems Using Exact Diagonalization. *Phys. Rev. B: Condens. Matter Mater. Phys.* **2015**, *92*, 045209.
(42) Magyar, R. J.; Tretiak, S. Dependence of Spurious Charge-Transfer Excited States on Orbital Exchange in TDDFT: Large Molecules and Clusters. *J. Chem. Theory Comput.* **2007**, *3*, 976−987.
(43) Dreuw, A.; Head-Gordon, M. Failure of Time-Dependent Density Functional Theory for Long-Range Charge-Transfer Excited States: The Zincbacteriochlorin−Bacteriochlorin and Bacteriochlorophyll−Spheroidene Complexes. *J. Am. Chem. Soc.* **2004**, *126*, 4007−4016.
(44) Magyar, R. J.; Tretiak, S. Dependence of Spurious Charge-Transfer Excited States on Orbital Exchange in TDDFT: Large Molecules and Clusters. *J. Chem. Theory Comput.* **2007**, *3*, 976−987.
(45) Ernzerhof, M.; Scuseria, G. E. Assessment of the Perdew−Burke−Ernzerhof Exchange-Correlation Functional. *J. Chem. Phys.* **1999**, *110*, 5029−5036.

DOI: 10.1021/acs.jpca.8b03481
J. Phys. Chem. A 2018, 122, 7514−7521

(46) Adamo, C.; Barone, V. Toward Reliable Density Functional Methods without Adjustable Parameters: The PBE0Model. *J. Chem. Phys.* **1999**, *110*, 6158−6170.
(47) Becke, A. D. Density-functional Thermochemistry. III. The Role of Exact Exchange. *J. Chem. Phys.* **1993**, *98*, 5648−5652.
(48) Stephens, P. J.; Devlin, F. J.; Chabalowski, C. F.; Frisch, M. J. Ab Initio Calculation of Vibrational Absorption and Circular Dichroism Spectra Using Density Functional Force Fields. *J. Phys. Chem.* **1994**, *98*, 11623−11627.
(49) Krukau, A. V.; Vydrov, O. A.; Izmaylov, A. F.; Scuseria, G. E. Influence of the Exchange Screening Parameter on the Performance of Screened Hybrid Functionals. *J. Chem. Phys.* **2006**, *125*, 224106.
(50) Muscat, J.; Wander, A.; Harrison, N. M. On the Prediction of Band Gaps from Hybrid Functional Theory. *Chem. Phys. Lett.* **2001**, *342*, 397−401.
(51) Brothers, E. N.; Izmaylov, A. F.; Normand, J. O.; Barone, V.; Scuseria, G. E. Accurate Solid-State Band Gaps via Screened Hybrid Electronic Structure Calculations. *J. Chem. Phys.* **2008**, *129*, 011102.
(52) Broqvist, P.; Alkauskas, A.; Pasquarello, A. Hybrid-Functional Calculations with Plane-Wave Basis Sets: Effect of Singularity Correction on Total Energies, Energy Eigenvalues, and Defect Energy Levels. *Phys. Rev. B: Condens. Matter Mater. Phys.* **2009**, *80*, 085114.
(53) Paier, J.; Marsman, M.; Kresse, G. Dielectric Properties and Excitons for Extended Systems from Hybrid Functionals. *Phys. Rev. B: Condens. Matter Mater. Phys.* **2008**, *78*, 121201.
(54) Tsuneda, T.; Singh, R. K.; Nakata, A. On Low-Lying Excited States of Extended Nanographenes. *J. Comput. Chem.* **2017**, *38*, 2020−2029.
(55) Frisch, M. J.; Trucks, G. W.; Schlegel, H. B.; Scuseria, G. E.; Robb, M. A.; Cheeseman, J. R.; Scalmani, G.; Barone, V.; Petersson, G. A.; Nakatsuji, H.; et al. *Gaussian 16*, revision B.01; Gaussian Inc.: Wallingford, 2016.
(56) Nicholls, R. J.; Morris, A. J.; Pickard, C. J.; Yates, J. R. OptaDOS - a New Tool for EELS Calculations. *J. Phys. Conf. Ser.* **2012**, *371*, 012062.
(57) Morris, A. J.; Nicholls, R. J.; Pickard, C. J.; Yates, J. R. OptaDOS: A Tool for Obtaining Density of States, Core-Level and Optical Spectra from Electronic Structure Codes. *Comput. Phys. Commun.* **2014**, *185*, 1477−1485.
(58) Plummer, B. F.; Al-Saigh, Z. Y.; Arfan, M. Anomalous Fluorescence of Aceanthrylene: An Example of Second Excited State Emission (S2 → S0). *Chem. Phys. Lett.* **1984**, *104*, 389−392.
(59) Dosche, C.; Kumke, M. U.; Ariese, F.; Bader, A. N.; Gooijer, C.; Dosa, P. I.; Han, S.; Miljanic, O. S.; Vollhardt, K. P. C.; Puchta, R.; et al. Shpol'skii Spectroscopy and Vibrational Analysis of [N]-Phenylenes. *Phys. Chem. Chem. Phys.* **2003**, *5*, 4563−4569.
(60) Peintinger, M. F.; Vilela Oliveira, D.; Bredow, T. Consistent Gaussian Basis Sets of Triple-Zeta Valence with Polarization Quality for Solid-State Calculations. *J. Comput. Chem.* **2013**, *34*, 451−459.

DOI: 10.1021/acs.jpca.8b03481
J. Phys. Chem. A 2018, 122, 7514−7521